

AD-A198 768

AFGL-TR-88-0106

DTIC FILE COPY

(4)

**CAT Forecasting Using Transient
Turbulence Theory**

**William H. Raymond
Roland B. Stull**

**University of Wisconsin
CIMSS/Department of Meteorology
Madison, WI 53706**

20 February 1988

Scientific Report No. 1

APPROVED FOR PUBLIC RELEASE; DISTRIBUTION UNLIMITED

**AIR FORCE GEOPHYSICS LABORATORY
AIR FORCE SYSTEMS COMMAND
UNITED STATES AIR FORCE
HANSCOM AIR FORCE BASE, MASSACHUSETTS 01731-5000**

**DTIC
ELECTE
JUL 2 7 1988**

"This technical report has been reviewed and is approved for publication"


George Modica
Contract Manager


H. Stuart Muench
Acting Branch Chief

FOR THE COMMANDER


KENNETH R. HARDY
Acting Division Director

This document has been reviewed by the ESD Public Affairs Office (PA) and is releasable to the National Technical Information Service (NTIS).

Qualified requestors may obtain additional copies from the Defense Technical Information Center. All others should apply to the National Technical Information Service.

If your address has changed, or if you wish to be removed from the mailing list, or if the addressee is no longer employed by your organization, please notify AFGL/DAA, Hanscom AFB MA 01731-5000. This will assist us in maintaining a current mailing list.

Do not return copies of this report unless contractual obligations or notices on a specific document requires that it be returned.

Unclassified

SECURITY CLASSIFICATION OF THIS PAGE

Form Approved
OMB No. 0704-0188

REPORT DOCUMENTATION PAGE

4. REPORT SECURITY CLASSIFICATION Unclassified		1b. RESTRICTIVE MARKINGS	
5. SECURITY CLASSIFICATION AUTHORITY		3. DISTRIBUTION/AVAILABILITY OF REPORT	
6. DECLASSIFICATION/DOWNGRADING SCHEDULE		Approved for public release; distribution unlimited	
7. PERFORMING ORGANIZATION REPORT NUMBER(S)		5. MONITORING ORGANIZATION REPORT NUMBER(S)	
		AFGL-TR-88-0106	
8. NAME OF PERFORMING ORGANIZATION University of Wisconsin	6b. OFFICE SYMBOL (If applicable)	7a. NAME OF MONITORING ORGANIZATION Air Force Geophysics Laboratory	
9c. ADDRESS (City, State, and ZIP Code) CIMSS/Department of Meteorology Madison, WI 53706		7b. ADDRESS (City, State, and ZIP Code) Hanscom AFB Massachusetts 01731 - 5000	
10a. NAME OF FUNDING/SPONSORING ORGANIZATION	8b. OFFICE SYMBOL (If applicable)	9. PROCUREMENT INSTRUMENT IDENTIFICATION NUMBER F19628 - 87 - K - 0035	
10c. ADDRESS (City, State, and ZIP Code)		10. SOURCE OF FUNDING NUMBERS	
		PROGRAM ELEMENT NO. 62101F	PROJECT NO. 6670
		TASK NO. 10	WORK UNIT ACCESSION NO. DB
11. TITLE (Include Security Classification) CAT Forecasting Using Transient Turbulence Theory			
12. PERSONAL AUTHOR(S) William H. Raymond and Roland B. Stull			
13a. TYPE OF REPORT Scientific No. 1	13b. TIME COVERED FROM: 20Feb 87 TO 20Feb 88	14. DATE OF REPORT (Year, Month, Day) 1988 Feb. 20	15. PAGE COUNT 26
16. SUPPLEMENTARY NOTATION			
17. COSATI CODES		18. SUBJECT TERMS (Continue on reverse if necessary and identify by block number)	
FIELD	GROUP	SUB-GROUP	Clear Air Turbulence (CAT) Turbulence parameterization Boundary Layer Surface Fluxes
19. ABSTRACT (Continue on reverse if necessary and identify by block number)			
<p>→ A transient turbulence parameterization has been inserted into the Penn State/NCAR regional three dimensional mesoscale numerical model. Transient turbulence parameterizes both boundary layer and clear air turbulence (CAT). The new transient turbulence scheme replaces separate formulations of the boundary layer parameterization, dry convective adjustment, cumulus parameterization and horizontal diffusion. A new surface layer flux formulation that is compatible with the transient turbulence parameterization has also been installed. Additionally a sixth order implicit tangent filter has been inserted to remove numerical noise. This separation of the turbulence physics from numerical stability considerations gives us an opportunity to examine the mixing process in greater detail.</p> <p>We compared forecasts from our revised model with the standard Penn State/NCAR model formulation, which has a Blackadar boundary layer and fourth order K theory horizontal diffusion. Forecasts using both Kuo cumulus parameterization and explicit cloud convective representations have been made with this standard model utilizing the OSCAR IV data set.</p>			
20. DISTRIBUTION/AVAILABILITY OF ABSTRACT <input type="checkbox"/> UNCLASSIFIED/UNLIMITED <input type="checkbox"/> SAME AS RPT. <input type="checkbox"/> DTIC USERS		21. ABSTRACT SECURITY CLASSIFICATION Unclassified	
22a. NAME OF RESPONSIBLE INDIVIDUAL George D. Madiga		22b. TELEPHONE (Include Area Code)	22c. OFFICE SYMBOL AFGL/LYP

(continuation of block 19)

Comparisons between the control and the transilient turbulence approach are used to highlight the role of turbulence and its affect on the overall forecast. Verifying station radiosonde reports and analysis are the final authority on the accuracy of the forecasts.

Our early results suggests that we should experience some positive benefits in the boundary layer forecasts once we have tuned the surface flux calculations. Turbulence at higher levels is also predicted in our forecasts. We plan to verify the existence of this turbulence against both CAT and turbulence in storm systems.

Table of Contents

	Page
1. Introduction	1
2. Transient Turbulence	2
a. The nonlocal nature of transient turbulence	
b. The closure procedure	
c. The numerical procedure	
3. Heat Flux With a Molecular Layer Included	5
4. The Implicit Tangent Filter	7
5. Discussion of Results	9
6. Conclusion and Future Activities	19
7. References	20



1. Introduction

Turbulence is a small-scale phenomena which cannot be resolved in large or mesoscale weather forecast models, but which affects the overall forecasts. The problem that faces the modeler is how to parameterize these turbulent motions within the constraints of time, money and computer power, while at the same time resolving scales many magnitudes larger.

The modelling of turbulence in the boundary layer and in the atmosphere above remains one of the more difficult problems in the atmospheric sciences. Sometimes turbulence and diffusion have been construed as the same process. In reality the processes involve different time and space scales and are physically different. Consequently, the first attempts to model turbulence (Boussinesq, 1877) took the diffusive formulation for the molecular viscosity of air, enhanced it, and called it an eddy viscosity. By specifying the eddy-diffusion coefficient in terms of known variables, the hydrodynamical equations of motion can be closed and solved. Attempts to find suitable parameterizations for the eddy viscosity based on bulk or large scale variables has occupied a predominate role in early meteorological boundary layer research. Following upon Boussinesq's constant eddy viscosity and Prandtl's (1925) mixing length theory, many complicated turbulence models have been proposed. In addition to K theory's first order closure scheme (Louis, 1979) there are higher-order closure formulations (Zeman, 1981; Wyngaard, 1982; Mellor and Yamada, 1982; Andre, et al., 1987) and spectral theories (Heisenberg, 1948) for turbulence.

In this report we turn our attention to the newly developed transilient turbulence parameterization (Stull, 1984). The nonlocal transilient turbulence parameterization has been compared with the above mentioned local approaches by Stull (1984, 1986) and to turbulent adjustment procedures by Stull and Hasegawa (1984). In many one dimensional tests (Stull and Driedonks, 1987; Stull and Kraus, 1987) this new formulation has yielded outstanding results.

The primary purpose of our investigation is to study the importance and predictability of turbulence in a three dimensional numerical model. In our testing we utilized the regional or limited-area Penn State/NCAR mesoscale model. Our philosophy is to replace separate formulations for K theory, dry convective adjustment, boundary-layer evolution and cumulus parameterization with one formulation, viz., the transilient turbulence. To accomplish our goals the Penn State/NCAR regional model had to be reformulated with the transilient turbulence parameterization scheme. All existing K theory coding was dismantled along with the dry and moist convective adjustment routines and the boundary-layer parameterization. A new surface flux procedure that was compatible with the new transilient turbulence parameterization was installed. It allows for a thin molecular layer

near the slab surface.

We selected the version of the Penn State/NCAR three-dimensional hydrostatic primitive equation mesoscale prediction model having fifteen vertical sigma levels (Anthes and Warner, 1978). In this model the horizontal grid included 61×46 points on a Lambert conformal mapping using a horizontal grid spacing of $\Delta x = \Delta y = 80$ km. Other model configurations include a nudging horizontal boundary condition and a two layer surface slab formulation. To remove numerical noise a 6th order implicit tangent filter (Raymond, 1988) was installed. This filter is very selective and enables numerical noise between $2\Delta x$ and $4\Delta x$ to be removed without altering meaningful meteorological scales. This allows the modeler a greater degree of freedom in testing turbulence parameterization schemes. The time step used is 120s.

Several 72 h forecasts have been ran and verification made for the OSCAR IV case (0000 UTC 22 April to 0000 UTC 25 April, 1981, prepared by NCAR, see Errico and Baumhefner, 1987). This data set represents a spring-time frontal situation in which cyclonic activity is located initially over the Dakotas and an upper-level trough exists just to its west. This system propagates eastward and intensifies, but several small scale waves are also present (Errico and Baumhefner, 1987). Additional cases will be tested in the near future but only the OSCAR case is presented in this first year report.

In the next section (2) we highlight the transilient turbulence parameterization. In section 3 we describe a surface flux scheme which contains a molecular layer modification while in section 4 the nature of the 6th order implicit filter is examined. Results from our calculations are presented in section 5. Section 6 summarizes our findings to date and talks about future activities.

2. Transilient Turbulence

a. The nonlocal nature of transilient turbulence

The transilient turbulence parameterization is a nonlocal first-order closure method that models the subgrid-scale mixing in the vertical (see Fig. 1). By nonlocal, we mean that mixing can occur between all pairs of grid points in a column during any one timestep, even if the points are not immediate vertical neighbors. Into each grid box of interest i , the fraction of air mixed from any other grid box j , during timestep Δt is represented by the transilient mixing coefficient $c_{ij}(t, \Delta t)$. The amount of tracer S carried with the air from box j to i is the product $c_{ij}(t, \Delta t) \cdot S_j(t)$.

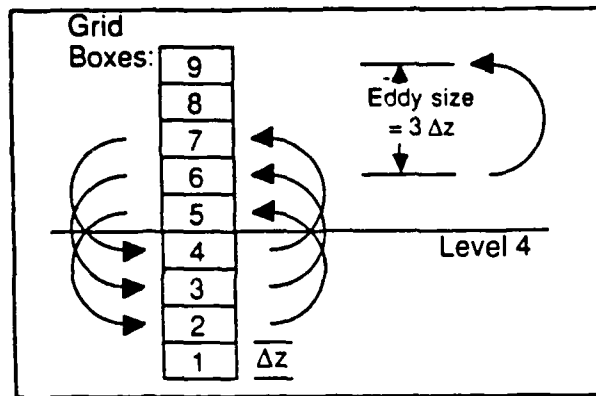


Fig. 1. Schematic showing grid boxes and flux levels. Only those eddies of size $3\Delta z$ that contribute to the flux across level 4 are shown.

The set of all coefficients describing mixing between every pair of points during one timestep is a matrix called the transilient matrix. The elements in each row and each column of the transilient matrix must sum to one, to insure air-mass and tracer-mass conservation. No element can be negative without violating the increase in entropy of mixing, thus each element must satisfy $0 \leq c_{ij} \leq 1$.

The forecast equation for a conservative tracer, considering only turbulence, is thus described by matrix multiplication (Stull and Driedonks, 1987):

$$S_i(t+\Delta t) = \sum_{j=1}^n c_{ij}(t, \Delta t) S_j(t). \quad (1)$$

This same equation is used to model turbulent mixing of heat, moisture, and momentum.

Fig. 2 shows how transilient matrices can be interpreted: the column index indicates from where the air is coming, and the row index indicates to where it is going. The element highlighted in Fig. 2a is in column 4 row 2, and represents the mixing from box 4 to box 2 shown in Fig. 2b. The arrow drawn in Fig. 2b is not a physical eddy, but instead represents the mixing process associated with a variety of eddies.

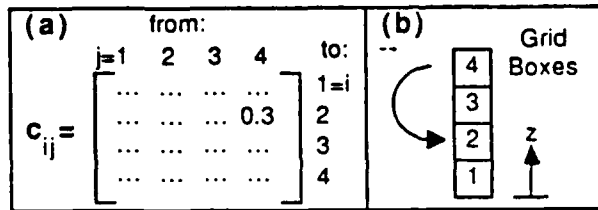


Fig. 2. Schematic (a) highlighting one element of a transilient matrix, and (b) indicating the associated mixing process between grid boxes in a column.

b. The closure procedure

Stull and Driedonks (1987) presented a closure procedure based on the turbulent kinetic energy equation. In this nonlocal closure scheme let Y_{ij} denote the 'mixing potential' between two boxes i and j . Y_{ii} is the potential for no mixing outside of grid box i . Then the transilient coefficients c_{ij} are defined by

$$c_{ij} = Y_{ij} / \| Y \| \quad \text{for } i \neq j, \quad (2a)$$

with

$$c_{ii} = 1 - \sum_{\substack{j=1 \\ j \neq i}}^n c_{ij} \quad . \quad (2b)$$

Here n denotes the number of grid points in the vertical (15 in the Penn State/NCAR model)

Following Stull and Driedonks (1987) the mixing potential is defined from the turbulent kinetic energy equation using three scaling parameters; a timescale of turbulence T_O , a dimensionless parameter R_C relating buoyancy to shear, and a dimensionless dissipation factor D , giving,

$$Y_{ij} = T_O \Delta t / (\Delta z)_{ij}^2 [(\Delta U)_{ij}^2 + (\Delta V)_{ij}^2 - (g/R_C \theta_{vi}) (\Delta \theta_v)_{ij} (\Delta z)_{ij}] - D \Delta t / T_O , \quad (3)$$

for $i \neq j$. Here U and V are the velocity components, θ_v the virtual potential temperature, g the gravitational constant while Δz_{ij} is the distance between the centers of boxes i and j . In our calculations $T_0=1000$ s, $R_c=.21$ and $D=1$. These values follow the suggestions given in Stull and Driedonks (1987). They found that T_0 should be between 100 and 1000 s. The lower value was best for neutral conditions in the boundary layer. R_c represents a critical Richardson number above which no turbulence takes place. D makes allowances for molecular viscosity mixing.

The internal mixing potential for box i defined by Y_{ii} is restricted to be as large as any of the elements in the same row. To avoid convective overturning we furthermore restrict that the mixing potential be nonincreasing, i.e., away from the main diagonal the mixing potential does not increase in magnitude within any row of the transilient matrix.

c. The numerical procedure

During each timestep, the above 1-D transilient method is applied to each column of the grid points in the model. In addition to performing the vertical mixing, the locations of turbulence (both in the boundary layer and aloft as clear air turbulence) are saved. These locations are then output as CAT regions. In addition, horizontal mixing (proportional to the depth of the vertical mixing) is applied to only those neighboring grid points that were turbulent. The net result is a quasi-3-D turbulence scheme that automatically forecasts boundary-layer evolution and patchy CAT.

3. Heat Flux With a Molecular Layer Included

The heat flux used in the surface layer turbulence calculations within the Penn State/NCAR model is computed from

$$H_s = -\rho c_p k u_* T_* \equiv -c_1 (\theta_a - \theta_s), \quad (4)$$

where T_* is given by

$$T_* = (\theta - \theta_s) / \ln(z_a/z_o - \psi_H). \quad (5)$$

The parameter ρ is the density, k is the von Karman constant, c_p is the specific heat of air

at constant pressure, θ_s is the potential temperature at the nominal height z_s while θ_a is the corresponding air potential temperature at the lowest model level z_a . The friction velocity, u_* , is expressed as

$$u_* = \text{Max}(kV/\ln(z_a/z_o - \psi_M), u_{*o}), \quad (6)$$

while over water the definition of u_* is changed to

$$u_* = (4 \times 10^{-4} V 2.55)^{0.5}, \quad (7)$$

where $u_{*o} = .1 \text{ ms}^{-1}$ and $V = (V_a^2 + V_c^2)^{0.5}$. Here V_a is the wind speed at height z_a and V_c is a convective velocity (Anthes et al., 1987). The roughness height is z_o . The nondimensional stability parameters ψ_H and ψ_M are a function of the bulk Richardson number (Anthes et al., 1987).

As will be shown below it is very important to include the molecular layer in the heat flux calculations. The molecular layer is of depth z_μ . The molecular heat flux at z_μ is defined by

$$H_{s\mu} = -\rho K_{H\mu} (T_s - T_g)/z_\mu = -c_2(\theta_s - \theta_g). \quad (8)$$

Here $K_{H\mu}$ is the molecular conductivity in air.

Solving for θ_s in eq. (8), substituting into Eq. (4) and requiring the molecular and turbulent heat fluxes to be identical in the surface layer, i.e., $H = H_s = H_{s\mu}$, yields

$$H = -c_1(\theta_a - \theta_g)(1 + c_1/c_2)^{-1} \approx -c_1 c_3(\theta_a - \theta_g) \quad (9)$$

The ratio c_1/c_2 is defined as

$$c_1/c_2 \equiv c_p k^2 V z_\mu / [K_{H\mu} \ln(z_a/z_o - \psi_M) \ln(z_a/z_o - \psi_H)] \quad (10)$$

For typical values of V , z_a , z_μ , z_o , e.g., $V=5 \text{ ms}^{-1}$, $z_a=50 \text{ m}$, $z_\mu=0.01 \text{ m}$ and z_o between 0.01 and 0.5, we obtain for $c_3 = (1 + c_1/c_2)^{-1}$ a range of values between 0.20 and 0.06. Consequently it is clear that the molecular layer reduces the heat flux, Eq. (9), by at least 80%. Its inclusion into the model shelters the calculations from unrealistic gradients

associated with very steep super adiabatic layer found at the surface during the day, and from the reverse situation at night. In our model runs we have fixed the value of c_3 at 0.2.

4. The Implicit Tangent Filter

The set of symmetric low-pass implicit tangent filters (Raymond, 1988) of order $2p$ are defined by

$$[S^{2p}]u_n^F + (-1)^p \epsilon [L^{2p}]u_n^F = [S^{2p}]u_n . \quad (11)$$

Here u_n^F is the filter variable while u_n is the unfiltered quantity. In Eq. (11) L^2u_n is the finite-difference analog of the second derivative of u at grid location n multiplied by the square of the grid step size, i.e., $L^2u_n = u_{n-1} - 2u_n + u_{n+1}$. Similarly, order $2p$ of the operator is analogous in the same way to a $2p$ derivative. The coefficients associated with the $(L)^{2p}$ operation are identical to those in the binomial expansion of $(a - b)^{2p}$. Also $S^2u_n = u_{n-1} + 2u_n + u_{n+1}$; consequently $(S/2)^2$ may be thought of as an averaging operator. The coefficients for $(S)^{2p}$ are the $2p$ row entries in Pascal's triangle.

The implicit formulation requires the inversion of a banded diagonally dominant matrix to determine the filtered set u_n^F for all n . For $p=1$ the filter utilized in Pepper, et al., (1979) is recovered. The filter parameter ϵ is varied to control the degree of filtering, i.e. $\epsilon=0$ gives no filtering while $\epsilon=1$ will reduce a $4\Delta x$ feature by fifty percent for any order $2p$. The characteristics of the low-pass implicit tangent filter are best illustrated by examining the amplitude response function.

Assuming a Fourier expansion for both u_n and u_n^F in Eq. (11) and forming the ratio of the amplitudes yield, after simplification, an amplitude response

$$F(\kappa) = [1 + \epsilon \tan^2 p(\kappa\delta/2)]^{-1} . \quad (12)$$

Here δ is the grid step distance while κ is the wave number. This response is the same as that given by the recursive tangent filters described in Otnes and Enochson (1978). However the implicit tangent filter is nevertheless much easier to work with because the coefficient weights are known and boundary conditions encountered in limited area modelling are easily handled in the implicit formulation. Tedium calculations are otherwise required to determine the coefficients of the recursive tangent filter (Otnes and

Enochson, 1978) and boundary conditions are not obvious.

In Fig. (3) the response of the filter is shown after 24 hrs (720 applications with $\epsilon=.0075$) and is compared with the 4th order K theory horizontal smoothing normally used in the Penn State/NCAR regional model. Note for wave number $6\Delta x$ that the responses are much closer to the unfiltered value of 1 when using the 6th order implicit filter, whereas the old smoothing operator removes almost all of these feature, especially when the maximum K value is used.

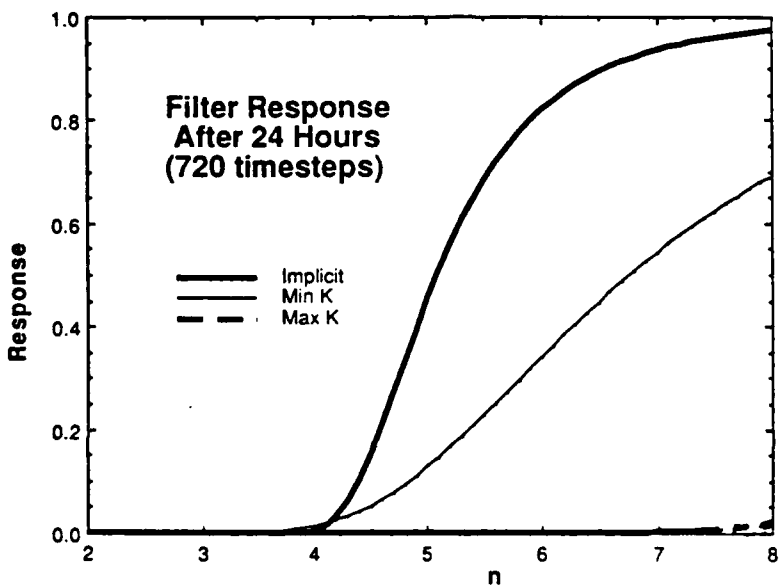


Fig. 3. The filter response verses wave length $n\Delta x$ after 720 applications for the implicit tangent filter and for the Penn-State/NCAR 4th order K theory diffusion.

In the model forecasts the filter, with $\epsilon=.0075$, is applied at every time step to the horizontal wind velocity components, the temperature and the mixing ratio fields. The filter parameter ϵ was selected to give the lowest acceptable smoothing while still maintaining stability and reasonable smooth fields. The application of the filter takes place after completion of the new time step and following the turbulence parameterization.

5. Discussion of Results

In Fig. 4 we illustrate for the OSCAR IV case the percent of the total number of horizontal grid points that contain turbulent exchanges, as a function of pressure and time, as predicted from a 72 hr forecast with the transilient turbulence parameterization. In Fig. 4 note that above the 500 mb level approximately one percent or less of the total number of the horizontal grid points are turbulent. The maximum at high levels occurs during the strongest cyclonic intensification which takes place between hours 18 through 48. In the lowest levels of the boundary layer more than 75% of the total horizontal grid points are turbulent during the peak heating in the diurnal cycle. Clearly there is a significant diurnal variation in the boundary layer.

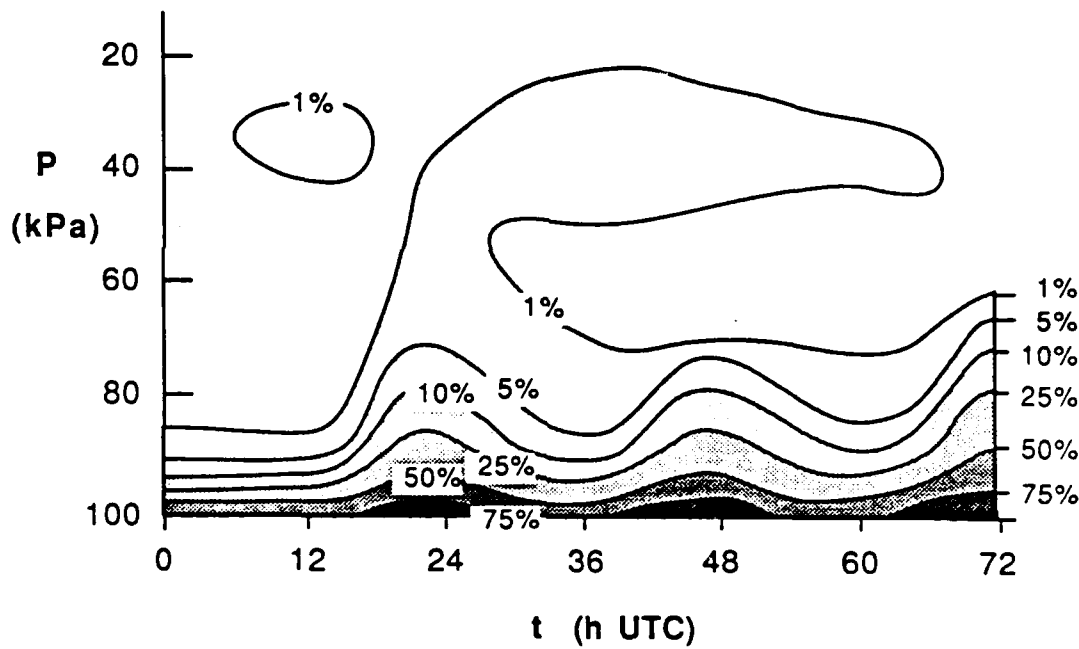


Fig. 4. The percent of the grid points turbulent as a function of time and pressure.

The horizontal distribution of turbulence in the boundary layer is shown in Figs. 5a,b. In Fig. 5a the distribution of the turbulence 21 hours into the forecast (near 3 pm local time) at $\sigma=0.94$ corresponds closely with the heated land mass. Only in the midwest (associated

with the major cyclonic activity) is there a turbulence free zone. This most likely occurs because of the stabilizing radiative and evaporative properties associated with the precipitating clouds. At higher levels in the atmosphere ($\sigma=.74$) the turbulence is confined to the mountainous regions as shown in Fig. 5b .

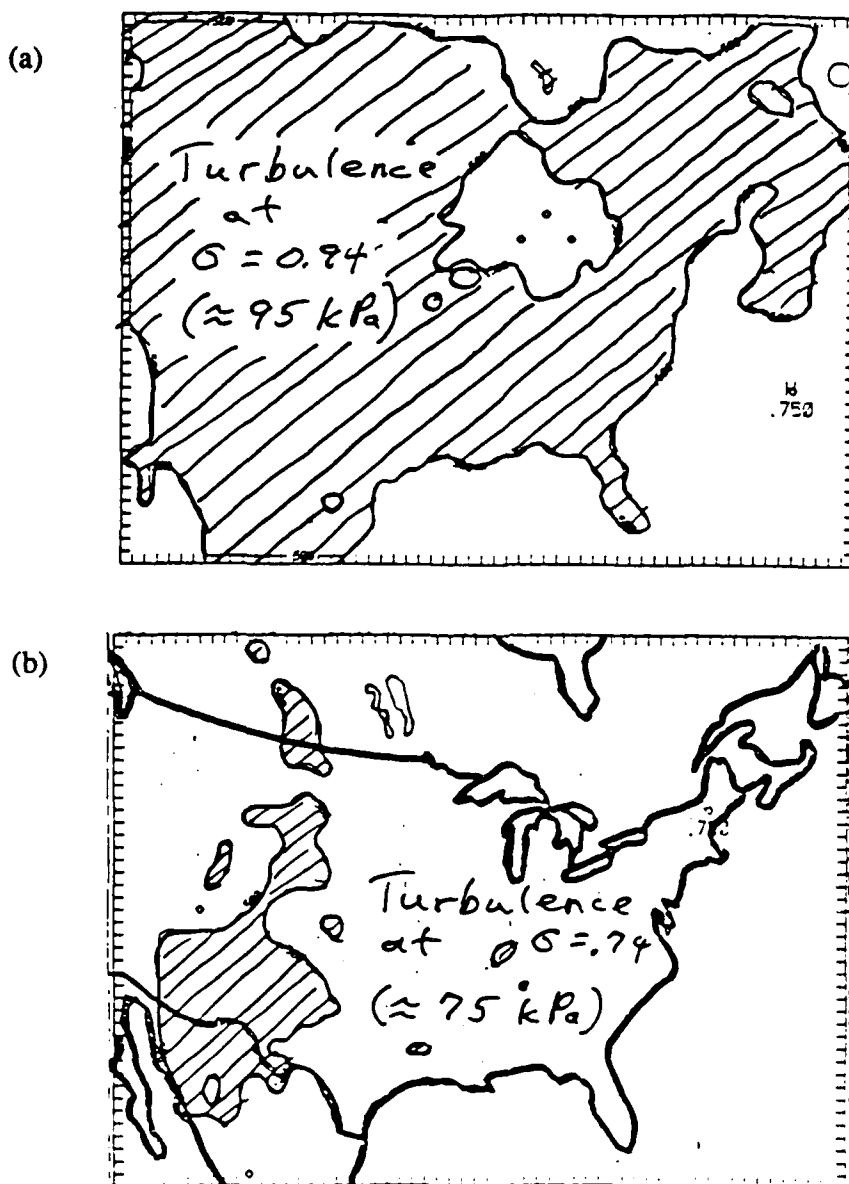


Fig. 5. The horizontal distribution of turbulence at (a) $\sigma=.94$ and (b) at $\sigma=.74$ twenty one hours into the forecast.

Vertical cross sections through the center of our region (taken west to east) are presented in Figs. 6a,b showing the potential temperature θ (K) and the mixing ratio (g kg^{-1}). Regions with turbulence are within or under the wide solid line found in the θ field in Fig. 6a. The turbulent boundary layer appears deepest over the mountains and just ahead of the front as shown between grid points 30 and 45, which is very realistic. Some turbulence is also occurring at mid-levels within the frontal zone above grid points 29 and 30. Note that some folding in the θ contours occur at mid levels between grid points 25 and 35 indicating the presence of the cold front. Clearly the largest amount of moisture is found in the warm sector. This is reflected in the contours of mixing ratio in Fig. 6b which have their greatest vertical extent between grid points 30 and 45.

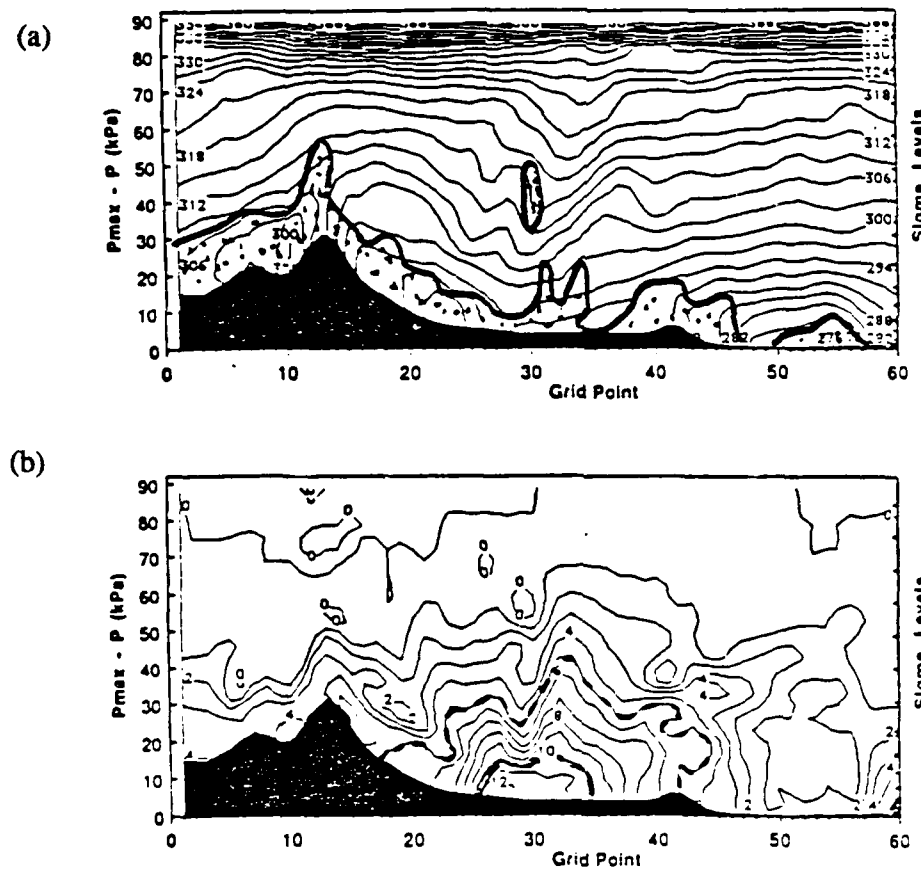


Fig. 6. Vertical cross sections of the (a) potential temperature (K) and (b) mixing ratio (g kg^{-1}). Turbulence indicated by the thick line and stipple in (a).

Fig. 7 shows the rms error at 850 mb for the forecast temperature. Results from four forecasts are displayed. The control run is the Penn State/NCAR model with the existing Blackadar boundary layer scheme and K theory horizontal diffusion. The control was ran with a Kuo cumulus parameterization and with an explicit cloud scheme, labeled (clouds) in Fig. 7. The transilient turbulence parameterization version was ran similarly except no cumulus parameterization was utilized in any of these computer simulations. Note in Fig. 7 that the rms errors, determined when forecast and radiosonde values are compared, are least for the transilient approach with explicit clouds, except near the end of the 72 hr forecast. Overall, carrying the clouds explicitly made little difference in these rms statistics.

RMS error in 850 mb forecast temperature .vs. radiosonde reports

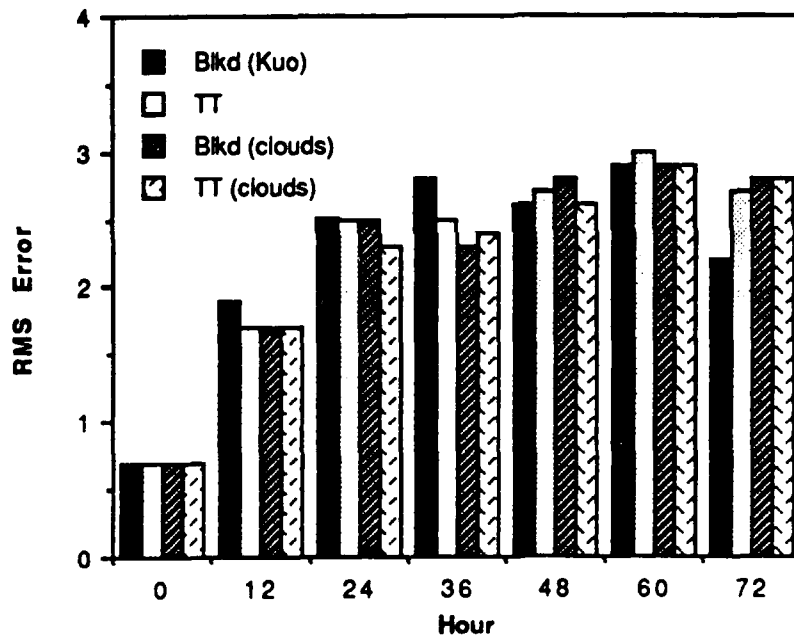


Fig. 7. The rms error in the 850 mb temperature for the control forecast, for the standard Penn State /NCAR package of the Blackadar boundary layer formulation with K theory, with the Kuo cumulus parameterization and with explicit clouds. Also illustrated is the transilient results with and without explicit clouds.

The effect of explicit clouds is however very clear in the mean error in the 850 mb temperatures shown in Fig. 8. Note that a change in sign is associated with whether the clouds are carried explicitly or not. The transient turbulence scheme has zero mean error at hours 12 and 24, and has the smallest mean error of the four forecasts. The control run, with and without explicit clouds, generally has much larger mean errors.

Mean error in 850 mb forecast temperature vs. radiosonde reports

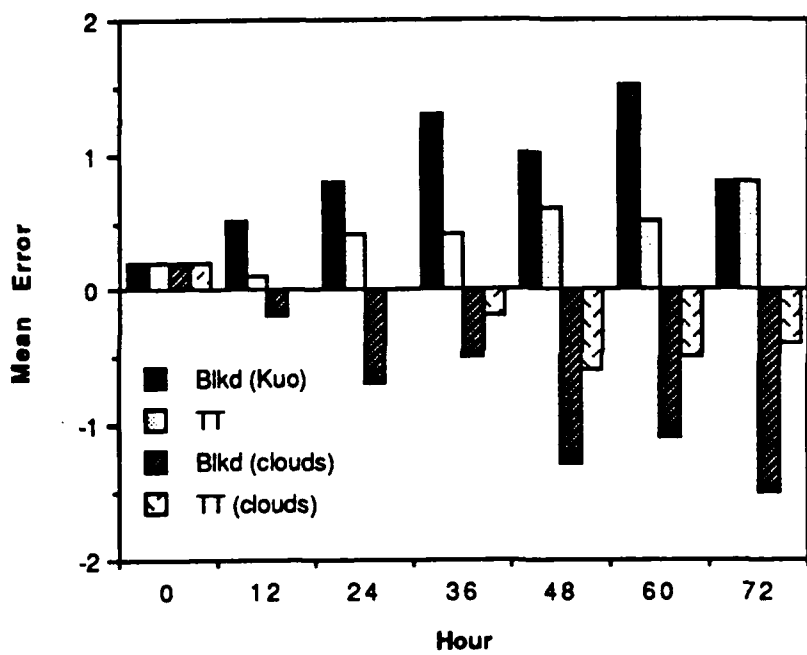


Fig. 8. Mean error for the cases displayed in Fig. 7.

Evidence is presented in Fig. 9 which shows that a systematic bias exists in the mean error for the 850 mb geopotential heights. Note that the control run with the Kuo cumulus parameterization has almost no mean error while the same control forecast made using an explicit cloud formulation has the largest error. Part of this error may be ascribed to inaccuracies in the forecasted phase velocity. However, evaporative and radiative feedback processes in the surface calculations are also of major importance. The error in the

transient turbulence approach suggests that the low-level forecast temperatures are too warm (approximately one degree). This is confirmed by comparing the temperatures predicted at the lowest sigma level (not shown). The geopotential height, being an integral of the virtual temperature retains errors that originate at the lower levels. In this regard we must scrutinize our new surface flux calculations and the surface flux balances to make sure we are getting the best solution, otherwise we can introduce biases into our forecast calculations. Additional testing still needs to be done in this regard.

Mean error in forecast 850 mb heights .vs. radiosonde reports

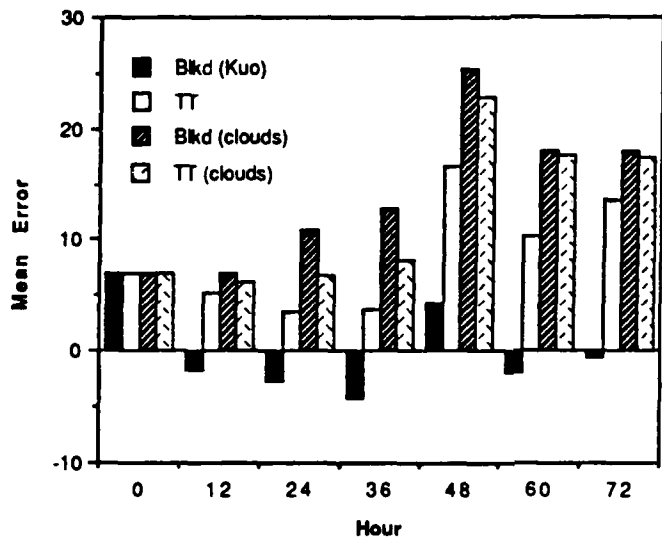


Fig. 9. Same as Fig. 8 except for the mean error in the 850 geopotential heights (m).

In Fig. 10 the mean sea-level pressure 48 hrs into the forecast is shown for the control runs, Kuo cumulus parameterization (10a), explicit cloud (10b), and for the transient version with explicit cloud (10c) and for the verification analysis (10d). Note that the low pressure centered over the great lakes is best represented in the transient forecast which has the correct pressure of 997 mb but over a reduced area as compared to the verifying analysis in Fig. 10d. The contraction of the surface low in the transient case is similar to the control case, with explicit cloud calculations, which has a central pressure of 996 mb. The control with the Kuo scheme has a 990 central pressure, so the low is deepened too much. As a consequence of this the 1008 pressure contour is however in a location closer to that indicated in the verifying analysis. Otherwise over most of the remaining area the control cases are slightly better by a small margin, but the presence of topography is a complicating factor making interpretation difficult.

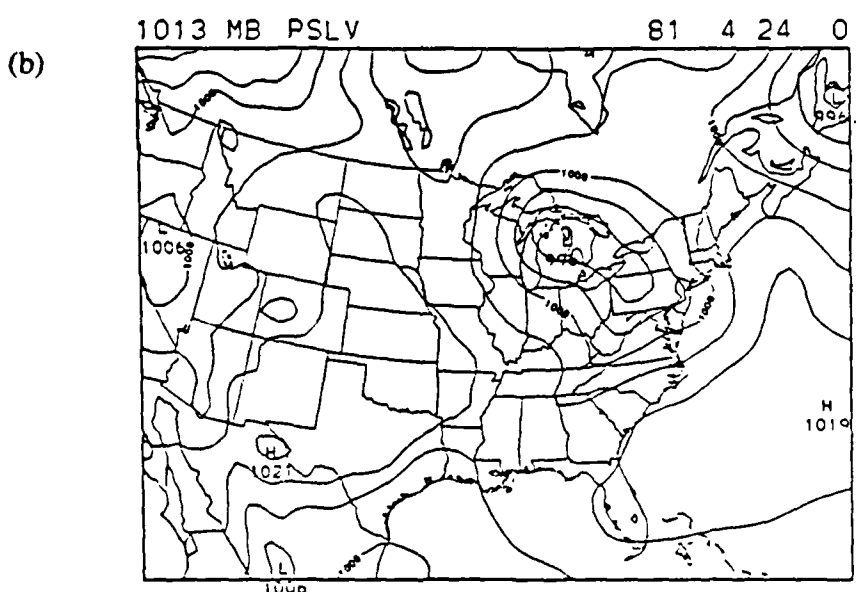
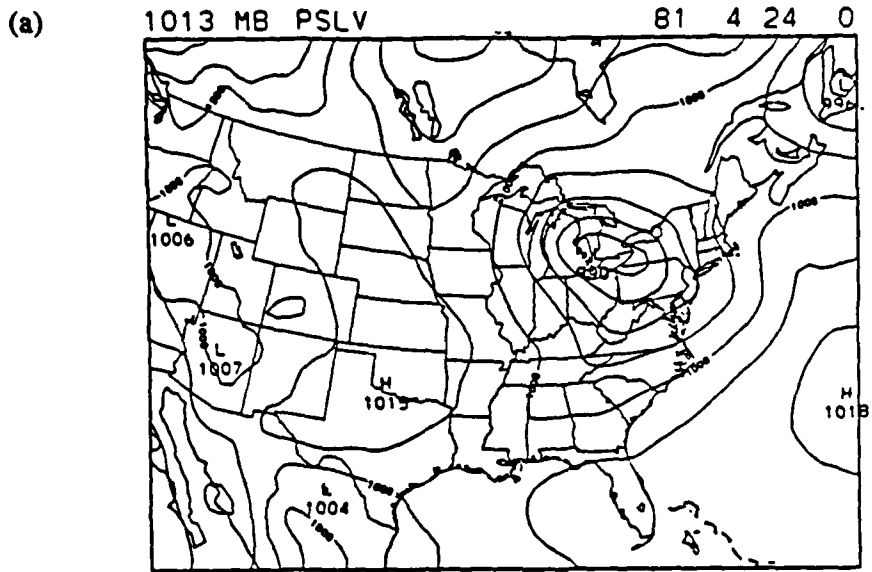


Fig. 10. Mean sea level pressure for (a) the control run with Kuo cumulus parameterization and (b) with explicit clouds. The transients turbulence parameterization scheme with explicit clouds is shown in (c). The verifying 48 h analysis is given in (d). Contour interval is 4 mb.

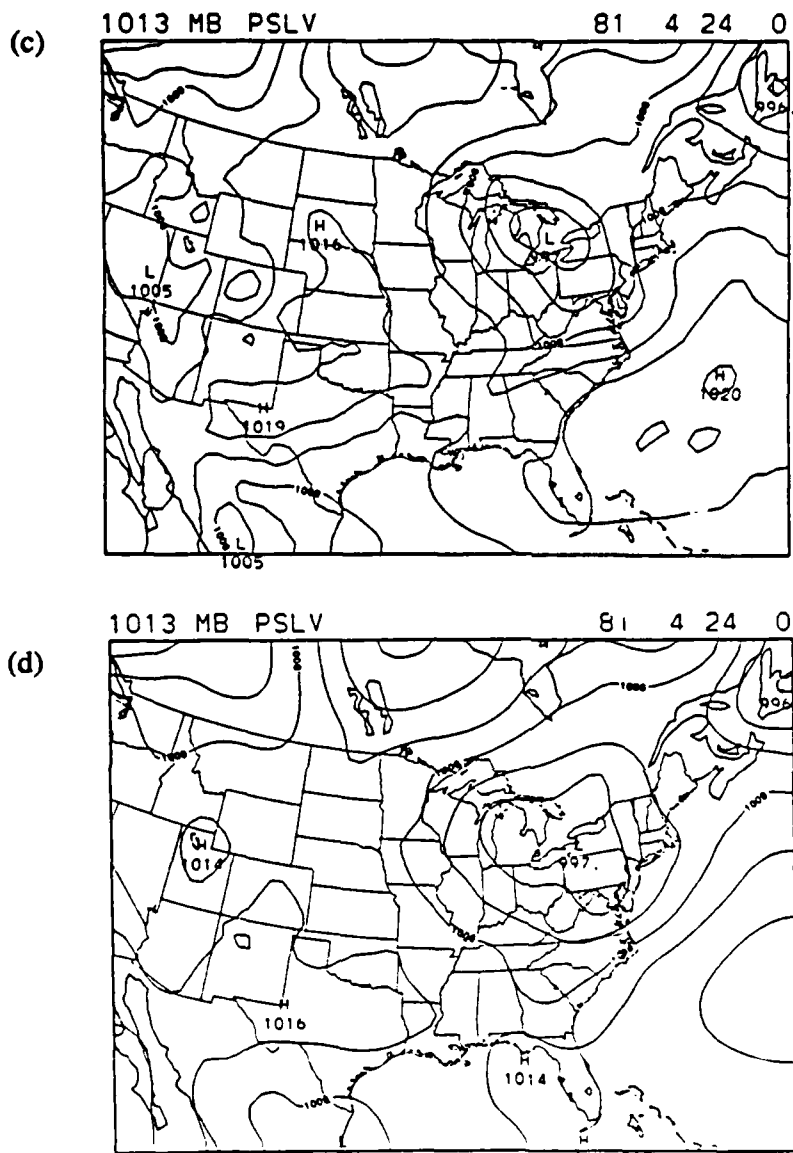


Fig. 10. Mean sea level pressure for (a) the control run with Kuo cumulus parameterization and (b) with explicit clouds. The transient turbulence parameterization scheme with explicit clouds is shown in (c). The verifying 48 h analysis is given in (d). Contour interval is 4 mb.

To gain some idea of the response at the surface we now turn our attention to Figs. 11a and 11b showing the surface slab or skin temperature, 48 hrs into the forecast at 0000 UTC 24 April, for the control case with Kuo cumulus parameterization and the equivalent transilient turbulence simulation. A comparison of these two figures shows that they are nearly the same in the north-eastern portion of our region while in the western part the skin temperature differences are up to 4 degrees in some locations. We expected and wanted slightly warmer surface skin temperatures in the transilient version. Remembering that the fluxes are being reduced by c_3 in Eq. (9), which compensates for the molecular layer, means that the overall heat flux felt by the lowest layer should be about the same as that observed in the control case.

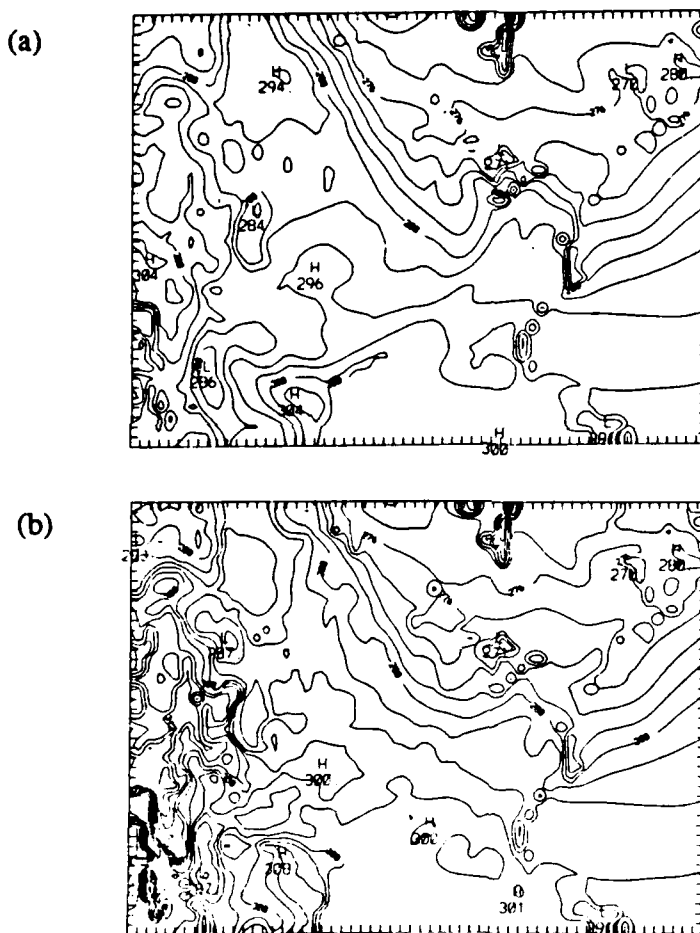


Fig. 11. The forecasted skin temperature, at hour 48, for the control (a) with the Kuo cumulus scheme, and for (b) the transilient turbulence formulation. Contour interval is 3 K.

Rainfall from the control and transilient 72 hr forecasts have about the same bias in all categories, as shown in Fig. 12, except for the last (2.64 cm) or largest rainfall accumulation. In the latter case note that all forecasts had a large positive bias. We believe this bias was enhanced for the transilient turbulence parameterization version because of two factors. The removal of K-theory horizontal diffusion increases the rainfall by the elimination of entrainment, because there is no horizontal mixing except where there is vertical mixing. Fig. 5 showed a significant turbulence-free zone in the boundary layer, induced, we believe, because of evaporative and radiative cooling associated with precipitating clouds (based on precipitation plots not shown). Additionally, the transilient approach tends to enhance boundary layer winds. Consequently, additional moisture is transported into the warm sector by the southerly component of the horizontal wind (not shown).

Bias scores (72 hrs) with and without explicit clouds

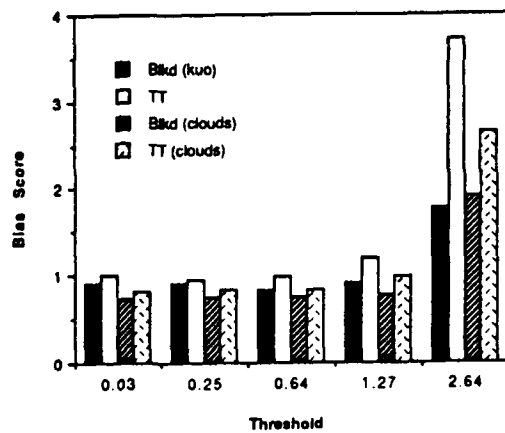


Fig. 12. Bias in the rainfall (cm) for the control, with Kuo or explicit clouds and for the transilient turbulence with or without explicit clouds.

Occasionally models have trouble with excessive condensation and/or overdevelopment as discussed by Zhang, et al. (1988). Such over development results in and is assisted by positive feedback mechanisms in latent heat release, moisture convergence and surface pressure decreases. Including realistic physics like evaporation and water loading reduces this problem (Zhang, et al., 1988). In our examination of the mean sea level pressure, Fig. 10, we saw that the transilient turbulence parameterization scheme did not cause excessive development in low pressure. Including the water loading, via explicit clouds, however did increase the accuracy of predicting the mean sea level pressure for both the transilient parameterization approach and for the control forecast.

6. Conclusions and Future Activities

We are very pleased that the transilient turbulence parameterization scheme does not cause the Penn State/NCAR regional model to become numerically unstable. We are also pleased with some of the early findings. In general we find that the new calculations are very similar to the control simulations. We believe that our statistics will improve when we have the new surface-layer flux scheme tuned correctly. Currently the lowest level temperature values are not now as accurate as they should be. This introduces a bias into the geopotential heights, as discussed in section 5, which gets carried throughout the entire depth of the model because the heights are calculated by an integral process. Our testing has taken somewhat longer than anticipated because of the number of parameters in the existing Penn State/NCAR surface flux parameterization to be tuned. We plan to complete all tests within the next two months.

We plan to examine the differences between standard-model forecasts made with cumulus parameterization and explicit cloud calculations against our improved model with and without explicit clouds. A detailed study of this type should be quite relevant and important for future attempts to adapt the transilient turbulence technique to cloud parameterization.

To date our testing of the transilient turbulence parameterization has utilized just one data set, i.e., the OSCAR IV case. As soon as we are satisfied that we are doing the best we can we will begin simulating other cases. We plan to make forecasts for at least six independent cases so that we can make some definitive statement regarding the accuracy, impact and desirability of the transilient turbulence parameterization scheme. We also want to get at least one data set that is less than five years old so that we can make comparisons between our forecasts of turbulence and the reports of CAT obtained from airplane pilots.

7. References

Andre, J.-C., G. DeMoor, P. Lacarrere, G. Therry and R. du Vachet, 1987: Modeling the 24-hour evolution of the mean and turbulent structures of the planetary boundary layer. *J. Atmos. Sci.*, 35, 1861-1883.

Anthes, R. A., and T. T. Warner, 1978: Development of hydrodynamic models suitable for air pollution and other mesometeorological studies. *Mon. Wea. Rev.*, 106, 1045-1078.

Anthes, R. A., E.-Y. Hsie, and Y.-H. Kuo, 1987: Description of the Penn State/NCAR Mesoscale model version 4 (MM4). NCAR technical note NCAR/TN-282+STR. 66 pp.

Boussinesq, J., 1877: Essai sur la theorie des eaux courantes. *Mem. pres. par div. savants a l'Academie Sci., Paris*, 23, 1-680.

Errico, R., and D. Baumhefner, 1987: Predictability experiments using a high-resolution limited-area model. *Mon. Wea. Rev.*, 115, 488-504.

Heisenberg, W., 1948: On the theory of statistical and isotropic turbulence. *Proc. R. Soc. London, Ser. A* 195, 402-406.

Louis, J. F., 1979: A parametric model of vertical eddy fluxes in the atmosphere. *Bound.-Layer Meteor.*, 17, 187-202.

Mellor, G. L., and T. Yamada, 1982: Development of a turbulence closure model for geophysical fluid problems. *Rev. of Geophy. and Space Phys.*, 20, 851-875.

Otnes, R. K., and L. Enochson, 1978: *Applied Time Series Analysis, Volume 1, Basic Techniques*. John Wiley & Sons, New York, 449 pp.

Pepper, D. W., C. D. Kern and P. E. Long Jr., 1979: Modeling the dispersion of atmospheric pollution using cubic splines and chapeau functions. *Atmos. Envir.*, 13, 223-237.

Prandtl, L., 1925: Bericht über Untersuchungen zur ausgebildeten. *Turbulenz. Z. ang. Math. Mech.* 5, 136-137.

Raymond, W. H., 1988: High-order low-pass implicit tangent filters for use in finite area calculations. Submitted to *Mon. Wea. Rev.*

Stull, R. B., 1984: Transient turbulence theory. Part I: The concept of eddy mixing across finite distances. *J. Atmos. Sci.*, 41, 3351-3367.

_____, 1986: Transient turbulence theory. Part III: Bulk dispersion rate and numerical stability. *J. Atmos. Sci.*, 43, 50-57.

Stull, R. B., and A. G. M. Driedonks, 1987: Application of the transient turbulence parameterization to atmospheric boundary layer simulations. *Bound.-Layer Meteor.*, 40, 209-239.

Stull, R. B., and T. Hasegawa, 1984: Transient turbulence theory. Part II: Turbulence adjustment. *J. Atmos. Sci.*, 41, 3368-3379.

Stull, R. B., and E. Kraus, 1987: The transient model of the upper ocean. *J. Geophys. Res.-Oceans*, 92, 10745-10755.

Wyngaard, J. C. 1982: Boundary layer modeling. In *Atmospheric Turbulence and Air Pollution Modelling*. Eds. F. T. M. Nieuwstadt and H. van Dop, Reidel, Dordrecht, Holland, 69-1061.

Zeman, O., 1981: Progress in the modeling of planetary boundary layers. *An. Rev. Fluid Mech.*, 13, 253-272.

Zhang, D.-L, E.-Y Hsie, and M. W. Moncrieff, 1988: A comparison of explicit and implicit predictions of convective and stratiform precipitating weather systems with a meso- β -scale numerical model. *Q. J. R. Meteorol. Soc.*, 114, 31-60.

END
DATE

FILMED

DTIC

11 - 88